Groundwater for Sustainable Development 26 (2024) 101307

Contents lists available at ScienceDirect

Groundwater for Sustainable Development

journal homepage: www.elsevier.com/locate/gsd

Research paper

Simulating the effects of retreating Urmia Lake and increased evapotranspiration rates on the nearby unconfined aquifer

Zahra Abdollahi [a,b], Bakhtiar Feizizadeh [b], Behzad Shokati [c], Mattia Gaiolini [d], Gianluigi Busico [e], Micòl Mastrocicco [e], Nicolò Colombani [d,*]

[a] Soil Conservation and Watershed Management Research Department, Zanjan Agricultural and Natural Resources Research and Education Center, AREEO, Zanjan, Iran
[b] Department of Remote Sensing and GIS, University of Tabriz, Tabriz, 51368, Iran
[c] Young Researchers and Elite Club, Maragheh Branch, Islamic Azad University, Maragheh, Iran
[d] SIMAU - Department of Materials, Environmental Sciences and Urban Planning, Marche Polytechnic University, Via Brecce Bianche 12, 60131, Ancona, Italy
[e] University of Campania "Luigi Vanvitelli", Department of Environmental, Biological and Pharmaceutical Sciences and Technologies (DiSTABiF), Via Vivaldi 43, 81100, Caserta, Italy

HIGHLIGHTS

- A MODFLOW-2005 model was developed in the North-eastern sector of Urmia lake.
- A transient model (2000–2016) was calibrated and validated versus hydraulic heads.
- MODIS dataset was used to identify trends of groundwater evapotranspiration.
- Urmia lake discharge in the aquifer decrease over time.

GRAPHICAL ABSTRACT

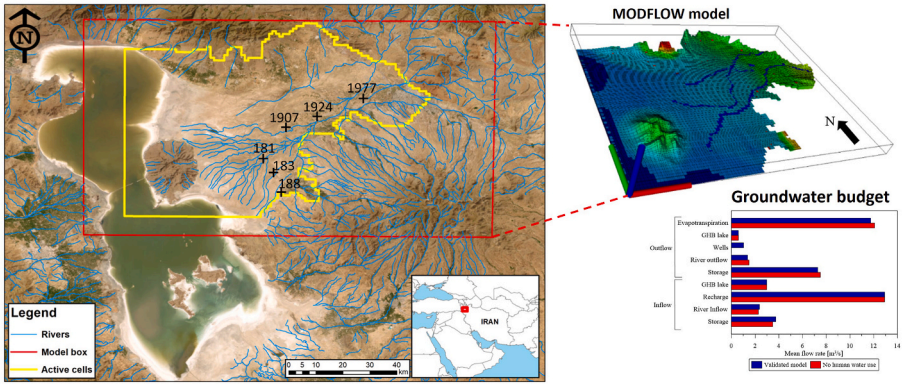

ARTICLE INFO

Keywords:
Numerical modelling
Groundwater flow
Remote sensing data
Evapotranspiration

ABSTRACT

The unsustainable management of water resources along with climate change impacts have led Urmia Lake to severely shrink since 1995. To quantify the groundwater losses in the surrounding area and to avoid the future worsening of a yet worrying scenario a numerical model is needed. For this purpose, a transient state MODFLOW model (2000–2016) has been calibrated and validated versus hydraulic heads. Good model performances were obtained, allowing to accurately estimate the groundwater budget. MODIS dataset was employed to set up the numerical model to identify temporal and spatial extent of evapotranspiration. Evapotranspiration turned out to play a massive contribution in groundwater outflow showing an increasing trend over time. Several scenarios, considering a different way to implement recharge and evapotranspiration in the modelling routine were assessed. The role of the spatialization of the evapotranspiration extinction depth was investigated by averaging remotely sensed heterogeneous datasets over the model domain. No significant differences in model performance

* Corresponding author.
E-mail address: n.colombani@univpm.it (N. Colombani).

https://doi.org/10.1016/j.gsd.2024.101307
Received 3 October 2023; Received in revised form 28 July 2024; Accepted 3 August 2024
Available online 5 August 2024

indicators were found. Moreover, a model scenario without human groundwater exploitation and land use change was considered. The results slightly differ from the groundwater budget calculated by the validated model and thus indicating the climate change as the major driver of groundwater depletion in the study area. The implementation of such a model allowed for the assessment of the exchange between the lake and the unconfined aquifer, providing a robust foundation for future sustainable management.

1. Introduction

Lake Urmia (LU), a hyper-saline lake in northwestern Iran, began shrinking in 1995 due to a combination of several factors such as: i) reduced rainfall, ii) rising temperatures, iii) dam-building, iv) extensive land-use changes, v) human settlements development, and vi) over-farming (Delju et al., 2013; Fathian et al., 2015). This led LU to lose almost 4000 km^2 of the lake surface from 1997 to 2018 (Pengra 2012; Tourian et al., 2015; Nasrollahi et al., 2021) and since it has no outlet to the sea, its shrinkage is primarily the result of evaporation and anthropic overexploitation. Consequently, a worrying decline in the LU water level has been registered leading to increasing salinity (Pengra 2012), which has reached values of more than 300 g/l during recent years, influencing the social, economic and cultural assets of the LU region (Eimanifar and Mohebbi 2007; Razzagh et al., 2021). In 2013 a restoration program was established and from 2017 the LU slowly recovered from its minimum extent due to a combination of man-made efforts and higher rainfall, with the latter recognized as the main driver (Nikraftar 2021).

During the past decades, the salinity of many large and permanent salt lakes has risen due to human activities (Williams 1993, 1996), and several have dried completely. Endorheic basins are inclined to be vulnerable to climate change, the most exemplifying case is the Aral Sea desiccation (Micklin 2010). These examples also include Owens Lake in California (Sharp and Glazner 1997), and Winnemucca Lake in Nevada (Williams 2001). In almost all cases, the reason for this desiccation is mainly due to the rerouting of inflowing rivers to meet agricultural and other human needs. Due to the drying up of LU, parts of the coastal aquifers have become salty, especially on the eastern shore of the lake. Due to excessive use of fertilizers, industrial development and intrusion of highly saline water from LU, the groundwater resources has experienced a worrying quality deterioration and quantity depletion (Schmidt et al., 2021). The East Azerbaijan province, located in the eastern shore of LU, is surrounded by very productive agricultural farmlands that produce food for 1.5 million inhabitants. Groundwater has been one of the main drinking, domestic, industrial, and agricultural water supplied in this area (Eimanifar and Mohebbi 2007). Recently, the number of wells has increased, and large volumes of groundwater are locally withdrawn, leading to a marked groundwater table decline over the past 20 years (Asghari Moghaddam and Allaf Najib 2006). Indeed, human activities related to improper management (Khazaei et al., 2019) and increasingly recurring meteorological droughts in the basin, have exacerbated groundwater decline over the last two decades (Kakahaji et al., 2013; Gholami et al., 2020; Yazdandoost et al., 2020). This has led to the increase in the phenomenon of salinization in both groundwater and lake water with consequential adverse effects on the regional ecosystems, agriculture, livelihoods, and health (Karbassi et al., 2010; Dehghanzadeh et al., 2015; Gholampour et al., 2015). Rising awareness and a better understanding of the lake behavior by the surrounding human population is vital to providing a foundation for future sustainable management of this endoreic lake (Eimanifar and Mohebbi 2007).

In this scenario, the development of numerical groundwater flow models become an essential step to properly investigate groundwater-related issues by evaluating trends of water fluxes over a simulation period. Since its release in 1988, MODFLOW has become the worldwide standard for groundwater modelling because of its flexible modular structure, complete coverage of hydrogeological processes, and free availability (Zhou and Li 2011). MODFLOW can also be integrated with a geographic information system (GIS) to provide a visual environment for groundwater resources evaluation and management (Aghlmand and Abbasi 2019). However, the lack of input data or the considerable spatial heterogeneity of specific parameters involved in the evaluation represent a notable challenge when simulating such complex hydrological systems (Kirubakaran et al., 2018). As indicated by Brunner et al. (2007), this paucity of data considerably limits the ability to assess, simulate, and manage surface and groundwater resources (Ntona et al., 2022), especially in semi-arid and arid environments with sparse and insufficient observations. Moreover, the use of conventional techniques, (e.g., geophysical, geostatistical techniques, numerical modeling, etc.) for groundwater management is often severely limited by the lack of adequate data and results to be expensive, laborious and time-consuming (Jha et al., 2007).

Recent developments in remote sensing have provided new opportunities to create spatially distributed input parameter sets for groundwater models and to constrain models during their calibration (Li et al., 2009). As an example, both Doble and Crosbie (2016) and Yao et al. (2015) emphasized that improvements in the reliability of groundwater models should be based on the validation of evapotranspiration by remote sensing data (Vasilevskiy et al., 2022). Despite the inclusion of both in situ and remote sensing observation datasets, recent efforts to calibrate and validate a hydrological model of the whole LU basin highlighted many sources of uncertainties and limitations, mainly related to coarse grid resolution and lack of hydrogeological information (Hosseini-Moghari et al., 2020).

In this study, a high-resolution grid groundwater flow model has been implemented via Processing Modflow 11 (Chiang, 2020), using specific remotely sensed data downloaded from national and worldwide databases. A transient simulation was carried out over a simulation period of sixteen years (2000–2016) and the model was validated against hydraulic heads at selected monitoring wells. This study aimed to quantify the LU aquifer connectivity and to investigate the impact of climate changes versus anthropogenic impact on groundwater resources via scenario modelling. To this regard the spatialization of the remotely sensed evapotranspiration extinction depth on both the model performances and the calculated evapotranspiration flow were assessed, since its massive contribution to the total output. In addition, the impact of spatialization of recharge rate was also assessed via scenario modeling.

2. Materials and methods

2.1. Characterization of the study area

The LU basin, known as one of the largest hypersaline water bodies on Earth, is located in north-western Iran (Fig. 1) and covers an area of about 52,000 km^2 (ULRP 2017). The lake lies amid the three provinces of West Azerbaijan, East Azerbaijan, and Kurdistan (Taheri et al., 2019). The basin hosts 5.2 million people, 50% of which live in East Azerbaijan province (Schmidt et al., 2021).

The LU basin is characterized by a cold semi-arid and Mediterranean Continental climate showing considerable seasonal variations in temperature, generally up to 40 °C in summer and between 0 and -20 °C in winter, with an annual mean of 12 °C (Mehrian et al., 2016). The annual precipitation varies between 300 and 400 mm, 77% of which occurs between December and May (Sima and Tajrishy 2013), while the annual evaporation rate from the surface of the lake is approximately 1000 mm

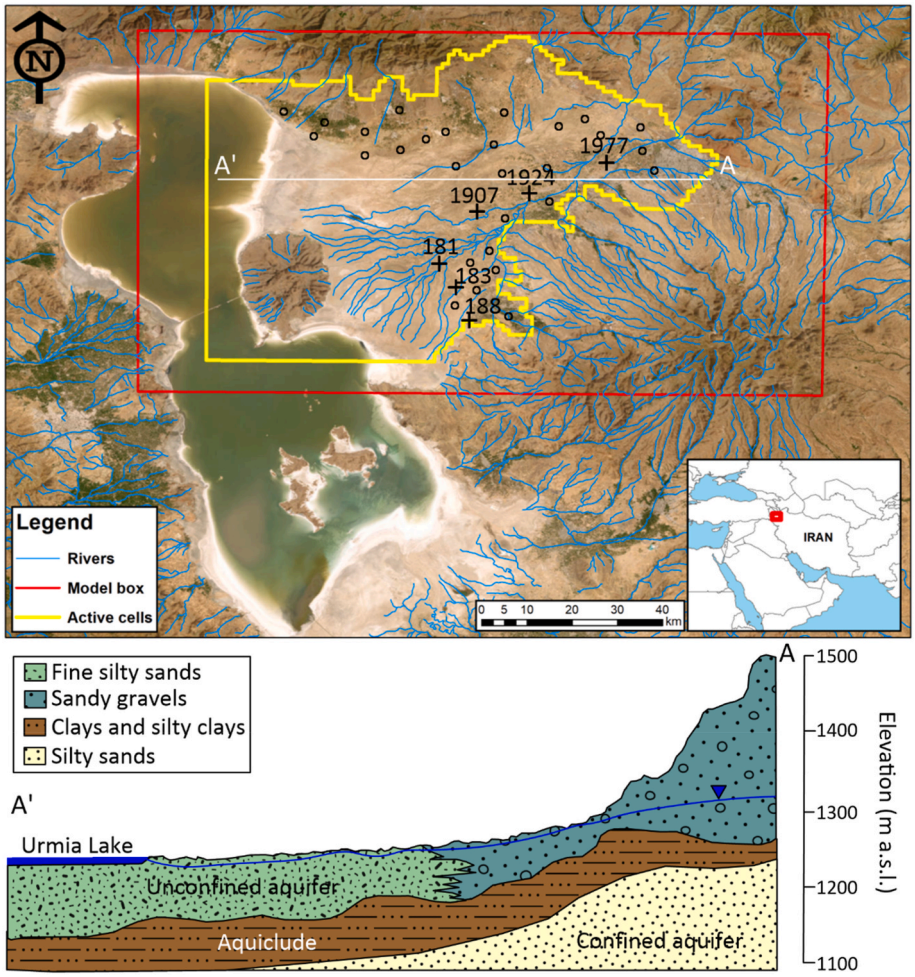

Fig. 1. Upper panel: model location, rivers, steady state monitoring wells (open circles) and transient monitoring wells (crosses). Lower panel: hydrogeological cross section with water table (blue line) and main hydrogeological units. (For interpretation of the references to colour in this figure legend, the reader is referred to the Web version of this article.)

(Taravat et al., 2016; Aschonitis et al., 2017; Agh, 2018). Summarizing, the LU basin can be classified as Dsa based on Köppen-Geiger's climate classification (Lotfirad et al., 2022).

From the geological point of view, the east of LU is made of four main geological units. The Permian Dorud and Ruteh formations which outcrop at west of Ajabshir, Triassic rocks are represented by the Elika formation consisting of limestone and dolomite outcropping in Maragheh and in Osku area, finally the Jurassic rocks outcrop at Kuh-e-Guyposhti and consists of 564 m of shale and sandstone (Alizadeh 2021). The Shemshak formation lies disconformably on the Elika formation in the east of LU. The Dalichay and Lar formations were deposited in a marine basin and consist of marl, sandstone, limestone, and dolomite. In the Maragheh area, the Jurassic units are covered by a Cretaceous basal conglomerate (up to 140 m) which contains pebbles derived from the Lar Formation. This unit grades up into a strongly folded flysch succession consisting of sandstone, shale, and intercalated volcanic rocks (Alizadeh 2021). Many thermal springs all over the basin testify the past volcanic activity (Feizizadeh et al., 2022). The Sabalan Volcano with a height of over 4810 m, consists of salt domes and volcanic ash rocks in Aji Chareh, and is one of the main geological features of northeastern Azerbaijan, northeast of the Tabriz fault (in the Alborz-Azerbaijan zone). The volcanic sedimentary rocks, such as travertine and young traces, host the aquifers that yield the primary source of groundwater (Heydarirad et al., 2019). In the northeast of the LU, the metamorphic rocks and Paleozoic platform sediments are bound by the Tabriz-Sofian-Bostan-Abad fault to the north and east (Mahmoudi et al., 2019). Salt clay is also observed around the lake (Radmanesh et al., 2022).

The unconfined aquifer consists of alluvial deposits formed by unconsolidated gravel, sand, and silty sediments deposited by streams, with an average thickness of 70–80 m (Fig. 1). Four hydrogeological units have been recognized from pumping test and stratigraphical logs with decreasing hydraulic conductivities from the hills to the central flat plain (Fig. 2). This is consistent with the diminishing energy of the depositional environment, which decreases the sediments grain size distribution. In this area, a confined aquifer is also present, but is not part of this study since the stratigraphical data are too sparse and pumping rates from wells are not always available.

2.2. Numerical model set up

The flow simulation was carried out using the MODFLOW-2005 code (Harbaugh 2005) and all the data were processed via Processing Modflow 11 to estimate groundwater flow budget. The equation that stands at the base of MODFLOW-2005 is the partial-differential equation that describes the three-dimensional movement of groundwater of constant density through a porous matrix:

$$\frac{\partial}{\partial x}\left(K_{xx}\frac{\partial h}{\partial x}\right)+\frac{\partial}{\partial y}\left(K_{yy}\frac{\partial h}{\partial y}\right)+\frac{\partial}{\partial z}\left(K_{zz}\frac{\partial h}{\partial z}\right)+W=S_s\frac{\partial h}{\partial t} \quad (1)$$

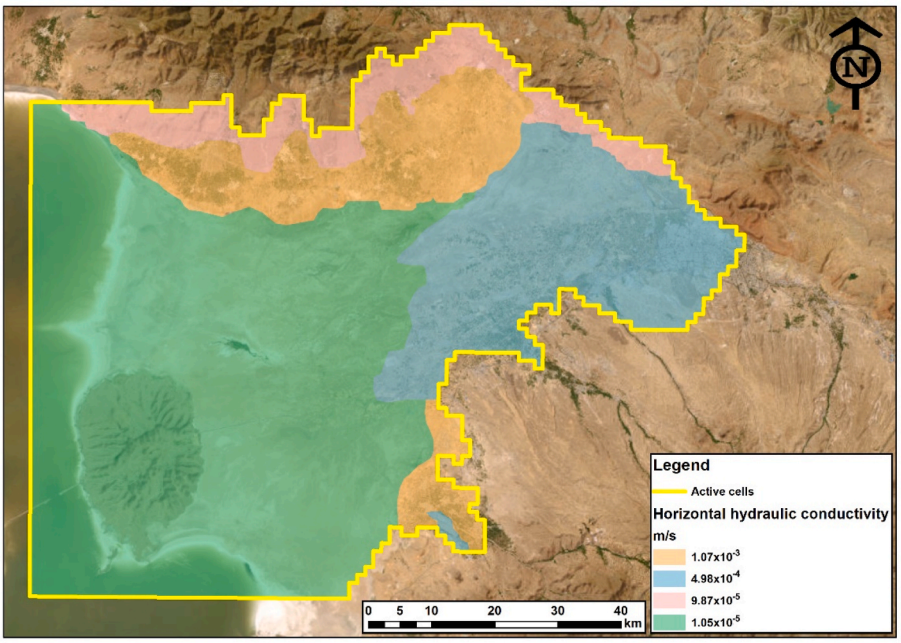

Fig. 2. Spatial distribution of the hydraulic conductivity upon study area.

where K_{xx}, K_{yy} and K_{zz} are values of hydraulic conductivity along x, y and z coordinate axes (LT^{-1}); h is the potentiometric head (L); W is a volumetric flux per unit volume representing sources and/or sinks of water (T^{-1}); S_s is the specific storage of the porous material (L^{-1}); and t is time (T).

The model domain consisted of 110 rows, 155 columns, and 1 layer with variable width and thickness, covering an area of 9600 km^2, of which approximately 4010 km^2 were active cells. The top of the grid represents the local ground surface, ranging from 1263 to 2893 m above sea level (a.s.l.) while the bottom of the grid represents the bottom of the aquifers, ranging from 1157 to 1983 m a.s.l.

Before the implementation of the groundwater flow model, a data consistency analysis has been performed to define the conceptual model of the study area. The SRTM Digital Terrain Model with a spatial resolution of 20 × 20 m cells was used to retrieve topographic information and represent morphology. The data files contain the elevation in a digital format, averaged on the model grid. Vegetation, buildings, and other cultural features were removed digitally, resulting in a proper terrain model. Values of hydraulic conductivity, corresponding to boreholes in the same cluster, have been averaged and imported via polygons input method to get a representative value for each geological formation in the study area (Fig. 2).

The horizontal hydraulic conductivity values range from $1x10^{-5}$ m/s where salt clay layers are present, to $1x10^{-3}$ m/s where highly fractured rocks are present. While Specific Yield ranged from 0.05 to 0.2. Moreover, it must be stressed, that local scale heterogeneities like intensively faulted zones and/or small lenses, have not been explicitly incorporated in this large-scale model and for the principle of parsimony in numerical modelling, a simpler representation was here adopted (Hill 2006). All the data about wells, including pumping rates, effective radius, screen length, and groundwater drawdown were retrieved from the Regional Water Company of East Azerbaijan Province and entered in the model through the Well Package (WEL). LU levels were retrieved from ULRP (2017) and inserted into the model by means of the General Head Boundary (GHB) Package. Historical satellite imagery sourced from Google Earth was incorporated into the model to reproduce the shrinking of the lake during the simulation time. The Moderate Resolution Imaging Spectroradiometer (MODIS) products have been questioned to obtain the trends of evapotranspiration in the study area for the period 2000–2016. Data were downloaded using the AppEEARS (AppEEARS Team 2020) interface and the MYD16A3GF model (Running et al., 2019) to obtain spatially interpolated values. Specifically, the spatial data representing the monthly evapotranspiration has been post-processed in GIS and aggregated in seasonal time steps for the whole considered period. The algorithm used in MODIS is based on the Penman-Monteith equation, which includes daily meteorological data along with remotely sensed variables, such as vegetation dynamics, albedo, and land cover (Mu et al., 2011). To derive a two-dimensional matrix representing the evapotranspiration extinction depth (Shah et al., 2007), land use and soil texture maps (Table 1) were overlapped in GIS environment. Namely, the evapotranspiration extinction depth is the distance from below the ground surface elevation where evapotranspiration from the water table ceases.

The precipitation values were retrieved from 10 meteorological stations provided by the General Meteorological Department of East Azerbaijan Province. The recharge values were spatially interpolated in the model domain by means of the Recharge Package multiplying precipitation values by a two-dimensional matrix representing the topographic factor. The Shepard (1968) weighted interpolation methods is used in Processing Modflow 11 (Chiang, 2022), which improves the pure inverse distance weighting method by adding functions to dynamically determine (1) the radius of influence based on data density and distribution, and (2) the weighting factors based on distance between model cells and data points in the interpolation algorithm.

The Processing Modflow polyline input method in the River Package was employed to simulate rivers, drawing their actual pathways, and

Table 1
National and worldwide open online datasets used to set up the model.

Dataset	Parameter	Repository	URL
Soil	Grain size distribution	ISRIC	https://maps.isric.org/
Geology	Aquifer thickness	This study	Upon request
Hydrogeology	Hydraulic conductivity	This study	Upon request
MYD16A3GF	Evapotranspiration rate	MODIS	https://doi.org/10.5067/MODIS/MOD16A2GF.006
	Recharge	This study	Upon request

defining river parameters. The riverbed conductance per unit length C_{rivl} (LT^{-1}), the river stage h_{riv} (L), and the elevation of the riverbed bottom B_{riv} (L) have been assigned to the most upstream and downstream vertices of each river polyline and then applied to the model cells employing a linear interpolation. Here only the 3 main surface rivers were simulated, while the other drainage channels visible in Fig. 1 are ephemeral water bodies that do not exchange water with the unconfined aquifer.

2.3. Model calibration and validation

Initially, a steady-state simulation has been processed and calibrated via PEST (Doherty 2010) using the data of the observed heads for the year 2000 at 39 selected wells distributed over the model domain. Assumed isotropic distribution of the K_{xx}, K_{yy} values was employed to avoid unnecessary long model runs and K_{zz} values were tied to K_{xx} in order to constrain the parameters estimation. For the steady-state simulation, both evapotranspiration and recharge rates were averaged for the year 2000 and interpolated on the numerical grid. Then, to investigate possible changes in the groundwater system associated with temporal variations of evapotranspiration and recharge patterns, a transient simulation was carried out over a simulation time of sixteen years (2000–2016). Sixty-eight stress periods of 3 months each (4 per year), additionally subdivided into 4 time steps, were used. The result of the steady state simulation was utilized as the reference starting hydraulic heads for the transient procedure as recommended by Harbaugh (2005). The validation of the transient state model was performed by exploiting the widespread network of monitoring wells measuring hydraulic heads (Fig. 1) over the simulation time to match modelled ones. Both the model calibration and validation were assessed by calculating the value of the coefficient of determination (R^2), the Nash-Sutcliff efficiency coefficient (NSE), and the mean absolute error (MAE). Finally, a global sensitivity analysis via PEST was performed, reporting the composite sensitivities for the transient model parameters.

2.4. Scenario modeling

Since the evapotranspiration pivotal role, once the model was calibrated and validated, a series of scenarios were considered to quantify the impact of data spatialization on the calculated evapotranspiration flow trends and averaged values, as well as on the model performance indicators. First, to analyze the role of the spatialization of the extinction depth (d) at the aquifer scale, mean (4.57 m) and median (5 m) values were applied to the whole domain in two simplified scenarios named d-Mean and d-Median, respectively. In addition, to vertically discretize the evapotranspiration rates along the model layer, the Evapotranspiration Segment Package (Banta, 2000) was used instead of the Evapotranspiration one (Scenario EVT-ETS1). This Package allows simulation of evapotranspiration with a user-defined relation between evapotranspiration rate and hydraulic head. The dependence of relative evapotranspiration (ratio of actual evapotranspiration to potential evaporation) on the depth of the groundwater table was assumed according to Vasilevskiy et al. (2022) for the desert areas.

A scenario using an average recharge rate over the entire domain was also tested versus the validated model to quantify the influence of this parameter on the groundwater budget calculation and on the model performance indicators.

The increasing anthropization that has affected the area in recent years has led to an increasing use of available water resources and land for drinking and agriculture use. To infer such a human impact, the anthropogenic pressure on both aquifer and soil was removed and the derived differences in piezometric levels and water balances were analyzed. To simulate this scenario no water exploitation from wells was considered and, since the extinction depth was derived from land use and soil texture maps, a new two-dimensional matrix was constructed and inserted into the model. Specifically, all those values of extinction depth related to anthropogenic land covers such as cultivated areas and settlement were replaced with values associated with bare lands. Only the values of pasture area were maintained similar to the previous scenario.

3. Results

3.1. Model performance and groundwater flow calculation

Fig. 3 shows the results of the calibration and validation phases for the calculated against the observed hydraulic heads in all the monitoring wells. Excellent model performances were achieved, resulting in both R^2 and NSE of 0.998 for the calibration and both R^2 and NSE of 0.993 for validation. MAE values (0.977 and 0.972 m, respectively) were judged satisfactory considering the wide range of the simulated piezometric levels (>100 m).

Besides, observations of groundwater levels from selected monitoring wells were used to verify the reliability of the model in describing water table fluctuations (Fig. 3).

The results highlighted some regions of the domain in the northern part of the model domain in correspondence of the Mishodagh Natural Reserve, characterized by high hydraulic gradient, while in the central zone hydraulic gradient drops following the topography of the region (Fig. 4).

The sensitivity analysis performed by PEST highlighted that the highest composite sensitivities are in the following order: recharge > evapotranspiration ≫ horizontal hydraulic conductivity of the zone near to the LU.

The model produced accurate estimates of the groundwater budget with a mean error of less than 0.05% among in and out components (Table 2). This allowed focusing on the single water budget components, whose fluxes are difficult to estimate without a physically based model even though they are crucial for better management of the hydrogeological basins.

The Processing Modflow ZoneBudget routine (Harbaugh 2005) allows for the calculation of the volumetric water budget in various parts of the model domain, accounting for storage, wells, rivers, lake, evapotranspiration, and recharge separately. Table 2 shows these components averaged over the simulation time in m^3/s, clearly revealing the massive contribution of the evapotranspiration (>50%) to the total groundwater output. Such an analysis indicates the evapotranspiration as one of the major causes of the groundwater to decline.

To highlight the impact of the LU's shrinkage on the surrounding aquifer, the calculated waterflow from the lake into the aquifer has been visually depicted in Fig. 5.

The waterflow from the lake into the aquifer exhibits a gradual decline throughout the simulation period according with historical satellite imagery sourced from Google Earth, while still retaining a seasonal variation. Notably, there is an exception during the initial four years of the simulation, where the trend remains relatively stable.

3.2. Scenario modelling assessment

To quantify differences amongst scenarios in the calculated evapotranspiration flow both graphically and numerically, trends and averaged values were plotted together (Fig. 6). The evapotranspiration flow seasonally varies with increasing fluxes over the warm seasons, reaching values up to 20 m^3/s. The validated model linear trend (dashed line) displays a slightly increase in the evapotranspiration flow over the simulation time. This increment perfectly reflects the stressing climate change framework of the region, representing a contributing factor to the drying condition and consequent increase in salinity of the LU (Delju et al., 2013).

As exemplified in Fig. 6, no significant changes occur between d-Mean, d-Median scenarios and the validated model. All the evapotranspiration flow trends are perfectly comparable (panel **a**) and the

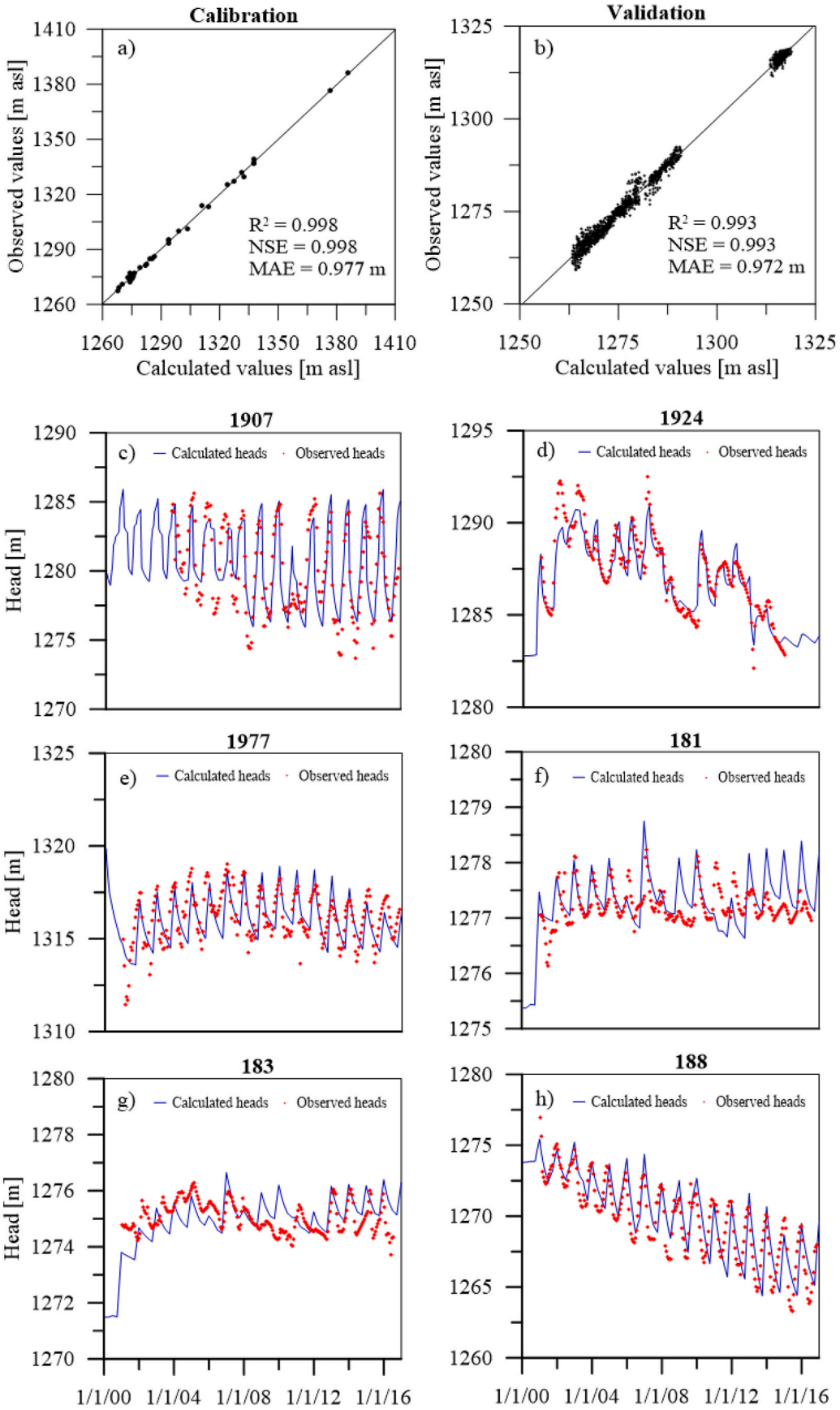

Fig. 3. Head Scatter Diagrams of the calibration (**a**) and validation (**b**) and comparison between calculated and observed hydraulic heads at selected monitoring wells (**c**–**h**), represented in Fig. 1.

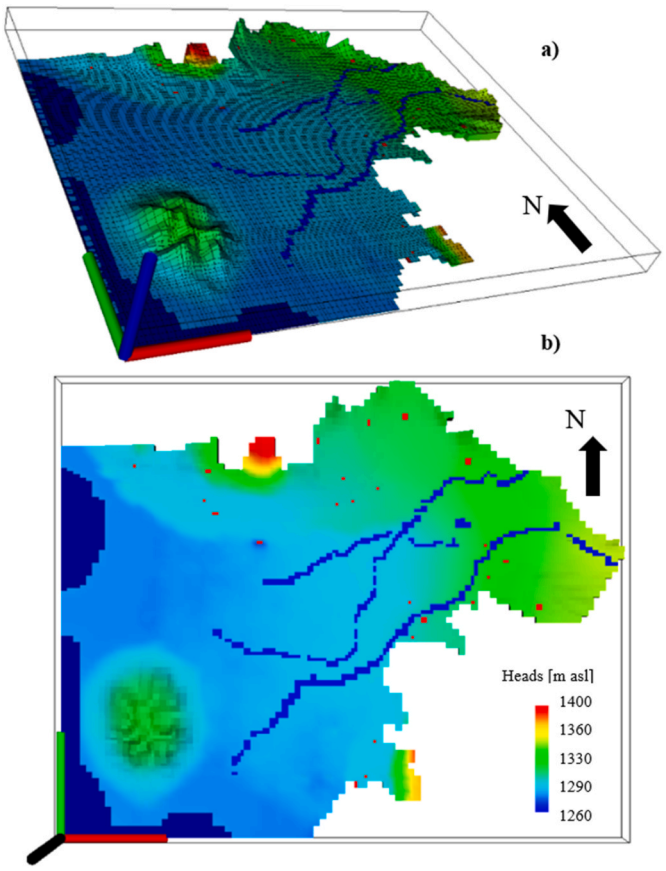

Fig. 4. Three-dimensional sketch (**a**) and planar view (**b**) of the calculated groundwater heads contour map at the end of the simulation.

Table 2
Component of the hydrogeological balance averaged over the simulation time.

Flow Term	IN (m^3/s)	OUT (m^3/s)	IN − OUT (m^3/s)
STORAGE	3.740	7.290	−3.550
WEL	0.000	1.024	−1.024
RIV	2.370	1.360	+1.011
EVT	0.000	11.75	−11.75
GHB lake	2.976	0.582	+2.394
RCH	12.93	0.000	+12.93
Sum	22.01	22.00	+0.01

differences between averaged values are negligible (panel **b**). Therefore, the spatialization of the evapotranspiration extinction depth over the domain could be avoided, saving operational and computational time. However, such spatialization should be considered in modelling very large and heterogeneous regions having a massive contribution to every groundwater budget component (Gaiolini et al., 2022).

Conversely, the application of the Evapotranspiration Segment Package, accounting for the dependence of relative evapotranspiration on the depth of the groundwater table, slightly affects the calculated evapotranspiration flow. In fact, the EVT-ETS1 scenario has produced both a reduced trend (red line in panel **a**) and averaged value (panel **b**). The vertical fractionation of the layer limiting the evapotranspiration rate according to the segmented function is the reason for such a reduction in the evapotranspiration flow.

The analysis of the model performance indicators confirmed that the spatialization of the evapotranspiration extinction depth could be overlooked. Specifically, all the model performance indicators (R^2, NSE, and MAE) resulted to be similar (Table 3). Nevertheless, the EVT-ETS1 scenario led to a slender decrease in both the R^2 and NSE indicators,

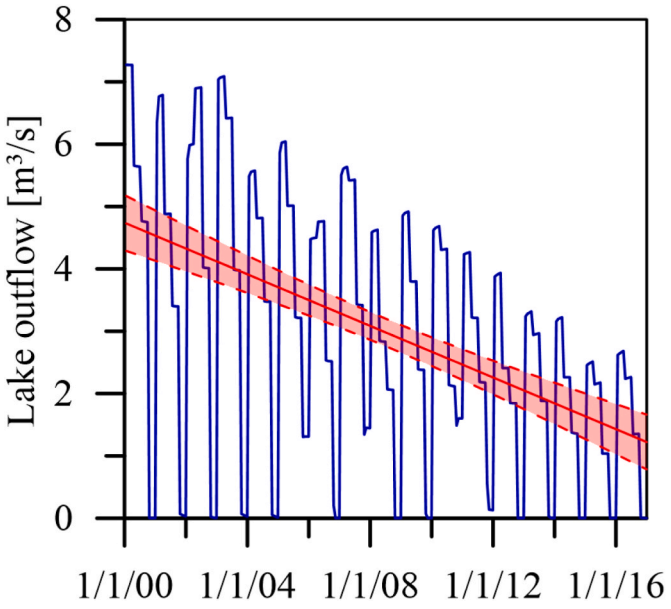

Fig. 5. Calculated lake outflow trend (solid blue line), linear trend (solid red line) and 95% confidence interval (dashed red lines) over the simulation. (For interpretation of the references to colour in this figure legend, the reader is referred to the Web version of this article.)

together with the MAE which has sharply increased. In Fig. 7 are shown the comparison of the flow budget using a spatially distributed recharge (Validated model) and the scenario with average recharge rate for each stress period (RCH-Mean). It is evident that using a mean recharge rate overestimated the model inflow during wet periods of up to 7 m^3/s and on average of 2 m^3/s which is a non-negligible overestimation of approximately 9% respect to the whole groundwater budget (see Table 2). Despite of this, only a minor decrease of the model performance indicators was recorded respect to the validated model (Table 3).

Finally, the scenario model without human water use was compared versus the results of the validated model. The comparison of the hydraulic heads at the selected monitoring wells shows that in the inhabited areas where the water resources are overexploited, differences in the water table are massive, in some points more than 10 m (Fig. 8).

However, such differences are quickly dissipated moving away from these areas. Even if differences in the hydraulic heads are considerably high at some monitoring wells, the hydrogeological balance does not differ consistently by running the model with or without human impact (Fig. 9). The comparison was performed on each component of the budget that was averaged over the 16 years monitoring period. By running the model without human water use, groundwater flow to rivers and LU has increased of 8.51% and 0.56%, respectively.

4. Discussions

Previous studies have highlighted the presence of both climate variations and anthropization on LU shrinkage, despite there is not an agreement about the relative contributions (e.g., Hassanzadeh et al., 2012; AghaKouchak et al., 2015; Alizade Govarchin Ghale et al., 2018; Chaudhari et al., 2018). Discrepancies are likely due to different methodology of analysis, data input, the considered periods and conceptual models used (Hosseini-Moghari et al., 2020). For this reason, in this study the shallow aquifer of the upper LU has been modelled for a sufficiently long-time span to infer among climatic and anthropization causes of groundwater depletion. The validated model allowed to analyze and quantify the most relevant stresses in different portions of the domain at different times, like pumping rates, LU variations, rivers aquifer interactions, recharge and evapotranspiration.

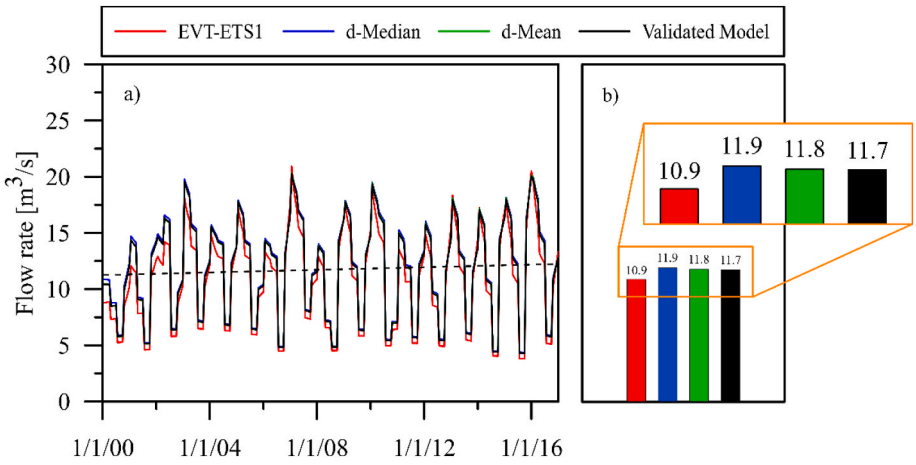

Fig. 6. Calculated evapotranspiration flow trends (**a**) and averaged values (**b**), and comparison between different scenarios. The dashed line represents the linear trend of the validated model.

Table 3
Model performance indicators: Coefficient of determination (R^2), Nash–Sutcliffe model efficiency coefficient (NSE) and Mean Absolute Error (MAE) for the different scenarios.

Scenario	R^2 (–)	NSE (–)	MAE (m)
Validated Model	0.993	0.993	0.972
d-Mean	0.993	0.993	0.972
d-Median	0.993	0.993	0.985
EVT-ETS1	0.992	0.987	1.430
RCH-Mean	0.991	0.987	1.309

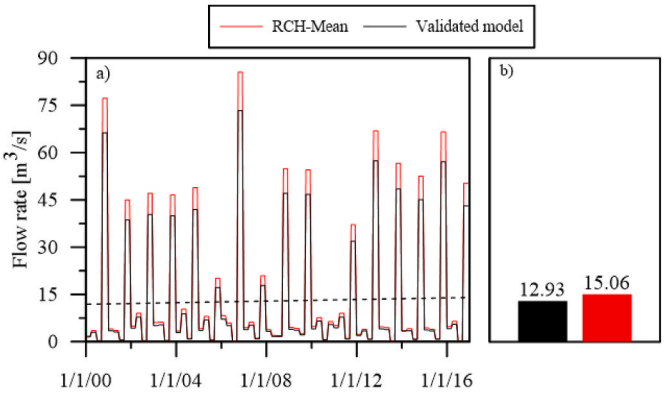

Fig. 7. Calculated recharge flow trends (**a**) and averaged values (**b**), and comparison between scenarios. The dashed line represents the linear trend of the validated model.

This study has demonstrated that the most important parameters in this portion of LU basin are: (i) recharge, (ii) evapotranspiration and locally (iii) pumping rates, compared to all the other stresses; and their impact on the model outcome is extremely high as witnessed by the model water budget and sensitivity analysis. These results agree with previous literature on large scale models (Condon et al., 2020; Doble and Crosbie 2016; Gaiolini et al., 2022) where the most striking and uncertain parameters are both evapotranspiration and recharge rates spatial and temporal variabilities. The key issue in optimization model development resulted to be the selection of spatial and temporal scale representing the system (Derepasko et al., 2021).

The model scenario technique helped to get insights on the latter topic, e.g., using a spatially averaged recharge rate highlighted that simplification of this highly spatially variable parameter can lead to misleading results given that it is affecting the groundwater budget but not the model performance based on groundwater level. Therefore, model uncertainty could only be diminished using independent flow observations (Rojas et al., 2010), but these are seldom available for aquifer scale models or often too coarse to be used as GRACE data (Forootan et al., 2014).

While often large-scale numerical models assumed no significant exchange between LU and the aquifer (Hosseini-Moghari et al., 2020); this numerical model is one of the first attempting to quantify the exchange rates among LU and the unconfined aquifer, which is non negligible in this area since the inflow from LU is more than 13% (see Table 2). In fact, the hydrologic connectivity between LU and nearby unconfined aquifer is still a topic that deserves more research as pointed out by Danesh-Yazdi and Ataie-Ashtiani (2019). In addition, given that the model assess that the flow is from the LU towards the aquifer, salinization of groundwater resources has to be expected. Moreover, the calculated evapotranspiration rate represents a contributing factor to the related salinization processes occurring in the area due to evapoconcentration (Tanji 2002). Unfortunately, there are no groundwater quality data to proof this hypothesis in the nearby vicinity of the LU and to calibrate a density dependent flow and transport model, but surely this would be matter of investigation in future studies. Moreover, the groundwater heads in the plain near to the UL where always above the maximum extinction depth of 5 m defined by Vasilevskiy et al. (2022), thus allowing a continuous outflow via evapotranspiration from groundwater, with minimum flow rates in winters and higher during summers. This is why the relative contribution of the various scenarios with different maximum extinction depths are so similar here. Again, whether the groundwater table is very deep or fluctuating among the maximum extinction depth, using different approaches may lead to different results.

It must be emphasized that the scenario modeling analysis was limited to the shallow groundwater system and no other surface water human stressors (i.e. dam-building and inflow river rerouting) have been considered, which possibly could lead to an underestimation of the human impact on LU shrinkage. In fact, Hosseini-Moghari et al. (2020) found that the overall human water resources overexploitation reduced LU during 2003–2013 by about 39%–45%. Moreover, they stressed that 87%–90% of groundwater storage loss was due to human water use, which is in contrast with the results achieved in this study. The reasons could be multiple and imputable to: the different areas under study, here only the shallow aquifer in the north-eastern sector of LU with an approximate area of 1514 km^2, while in the Hosseini-Moghari et al. (2020) study the whole LU basin was investigated with an approximate area of more than 66000 km^2; the model grid here is highly refined (on

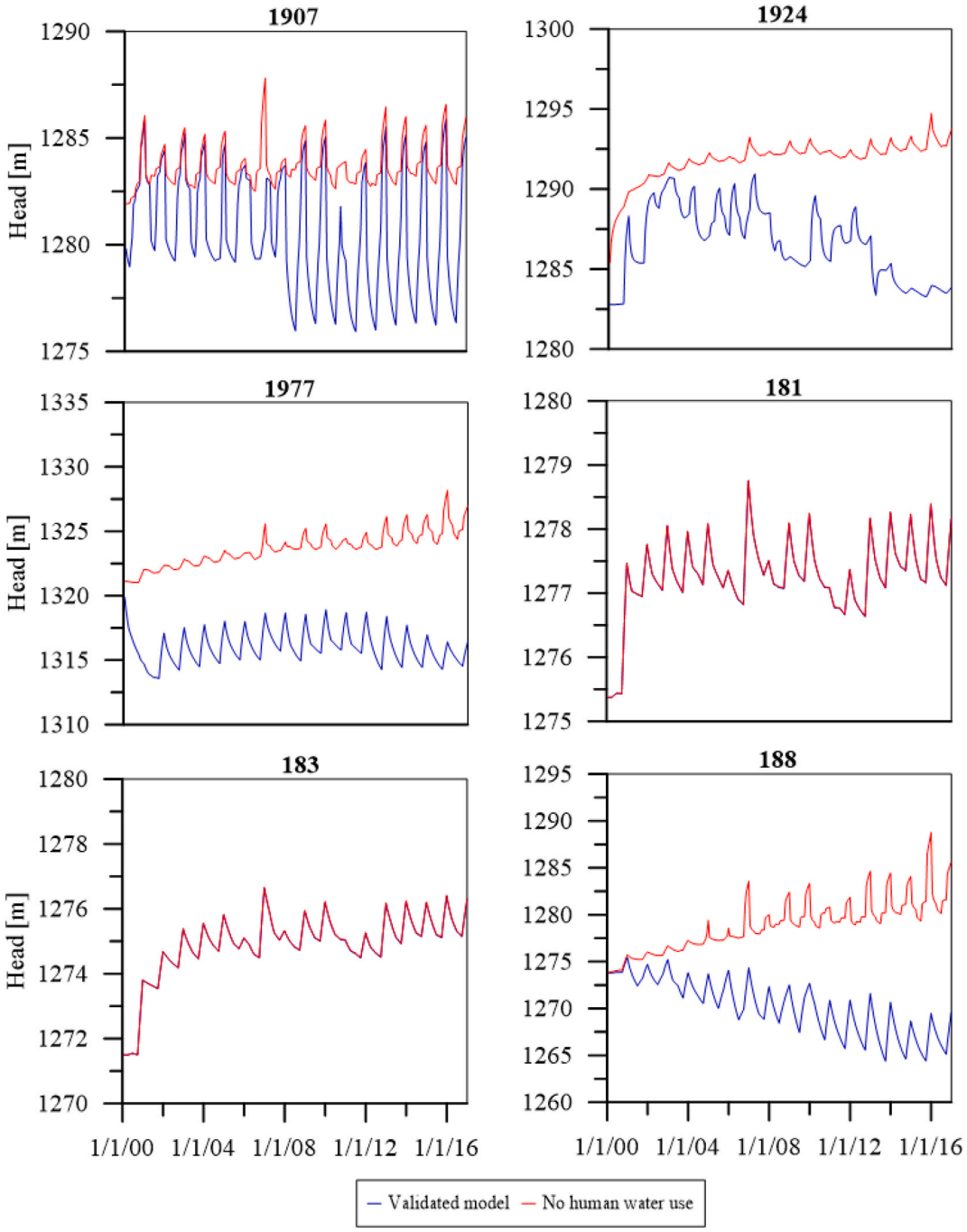

Fig. 8. Comparison between hydraulic heads at selected monitoring wells, represented in Fig. 1.

average 100 × 100 m), while in the Hosseini-Moghari et al. (2020) study was very coarse (0.5 × 0.5°); the pumping wells rate was very different since it included different overlayed aquifer systems and also the southern LU area which is more productive from an agricultural point of view.

Finally, as regards the climate change impact on the groundwater resources, this study is coherent with the results of Hosseini-Moghari et al. (2020) and also of Shadkam et al. (2016) which both found that the impact of climatic variations could not be ignored over the basin.

5. Conclusions

In this research, a steady-state and transient groundwater flow model was presented for LU, which demonstrated a good ability to describe groundwater fluctuations over simulation time and provided an accurate estimate of groundwater balance. The free available remote sensed products confirm to be valuable input data, especially in data scarce area, to correctly assess the role of evapotranspiration in groundwater balance. Specifically, the obtained results indicate the evapotranspiration as one of the major causes of the groundwater decline, along with human exploitation. In terms of data needs and effort and time employed to insert complex input data, using a high resolution spatialization of the recharge and extinction depth over the domain do not lead to significative better results in terms of model performance, but considerably affected the groundwater budget. The scenario without human stressor produced a significant water table increase at locations near to pumping wells, but no significative changes in the groundwater budget compared to the baseline scenario. This highlights that the

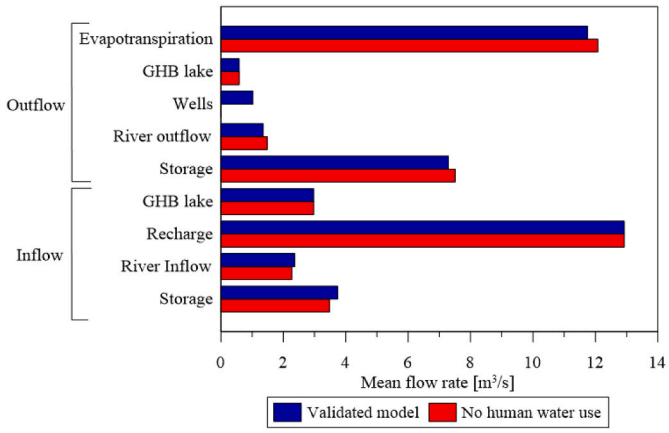

Fig. 9. Comparison between hydrogeological balance components averaged over the simulation time.

climate change has been the major driver of groundwater depletion in the study area. Future modelling considering expected water exploitation related to the land use management could help in better assess the weight of the human stress on both superficial and groundwater resources. The outcomes of the present study will help to gain a better understanding of the area and could represent an important tool to support decision making in water management for both agricultural and potable uses in the LU region.

Ethics approval

All authors kept the "Ethical Responsibilities of Authors".

Consent to participate

All authors gave explicit consent to participate in this study.

Consent for publication

All authors gave explicit consent to publish this manuscript.

Availability of data and materials

The data used to build up the model of this study are partially available on open datasets, while other are available from the corresponding author upon reasonable request.

Funding

This research was funded by University of Tabriz grant number [S4409]

CRediT authorship contribution statement

Zahra Abdollahi: Investigation, Formal analysis, Data curation. **Bakhtiar Feizizadeh:** Supervision, Investigation, Funding acquisition, Data curation. **Behzad Shokati:** Supervision, Resources, Project administration. **Mattia Gaiolini:** Writing – original draft, Visualization, Software, Investigation, Formal analysis. **Gianluigi Busico:** Visualization, Software. **Micòl Mastrocicco:** Writing – review & editing, Validation. **Nicolò Colombani:** Writing – review & editing, Software, Methodology, Conceptualization.

Declaration of competing interest

The authors declare that they have no known competing financial interests or personal relationships that could have appeared to influence the work reported in this paper.

Data availability

Data will be made available on request.

References

Agh, N., 2018. How to save lake Urmia. Presentation held in the premises of ULRP (Urmia Lake Restoration Program) regional office.

AghaKouchak, A., Norouzi, H., Madani, K., Mirchi, A., Azarderakhsh, M., Nazemi, A., Nasrollahi, N., Farahmand, A., Mehran, A., Hasanzadeh, E., 2015. Aral Sea syndrome desiccates Lake Urmia: call for action. J. Great Lakes Res. 41 (1), 307–311. https://doi.org/10.1016/j.jglr.2014.12.007.

Aghlmand, R., Abbasi, A., 2019. Application of MODFLOW with boundary conditions analyses based on limited available observations: a case study of Birjand plain in East Iran. Water 11, 1904. https://doi.org/10.3390/w11091904.

Alizade Govarchin Ghale, Y., Altunkaynak, A., Unal, A., 2018. Investigation anthropogenic impacts and climate factors on drying up of Urmia Lake using water budget and drought analysis. Water Resour. Manage. 32, 325–337. https://doi.org/10.1007/s11269-017-1812-5.

AppEEARS Team, 2020. Application for Extracting and Exploring Analysis Ready Samples; Ver. 2.54.1. NASA EOSDIS Land Processes Distributed Active Archive Center (LP DAAC). USGS/Earth Resources Observation and Science (EROS) Center: Sioux Falls, SD, USA. Available online: https://lpdaacsvc.cr.usgs.gov/appeears.

Aschonitis, V.G., Papamichail, D., Demertzi, K., Colombani, N., Mastrocicco, M., Ghirardini, A., Castaldelli, G., Fano, E.A., 2017. High-resolution global grids of revised Priestley-Taylor and Hargreaves-Samani coefficients for assessing ASCE-standardized reference crop evapotranspiration and solar radiation. Earth Syst. Sci. Data 9 (2), 615–638. https://doi.org/10.5194/essd-9-615-2017.

Asghari Moghaddam, A., Allaf Najib, M., 2006. Hydrogeologic characteristics of the alluvial tuff aquifer of northern Sahand Mountain slopes, Tabriz, Iran. Hydrogeol. J. 14 (7), 1319–1329. https://doi.org/10.1007/s10040-006-0036-1.

Banta, E.R., 2000. MODFLOW-2000, the U.S. Geological Survey Modular Ground-Water Model—Documentation of Packages for Simulating Evapotranspiration with a Segmented Function (ETS1) and Drains with Return Flow (DRT1). U.S. Geological Survey, Denver, CO [Report] = Open-File Report 00–466.

Brunner, P., Franssen, H.J.H., Kgotlhang, L., Bauer-Gottwein, P., Kinzelbach, W., 2007. How can remote sensing contribute in groundwater modeling? Appl. Hydrogeol. 15, 5–18. https://doi.org/10.1007/s10040-006-0127-z.

Chiang, E., 2020. Processing Modflow version 11.0.3: a graphical user interface for MODFLOW, gsflow, modpath, MT3D, PEST, seawat, and ZoneBudget. Simcore software. Last update july 4, 2022. In: https://www.simcore.com/wp/processing-modflow-11/.

Chaudhari, S., Felfelani, F., Shin, S., Pokhrel, Y., 2018. Climate and anthropogenic contributions to the desiccation of the second largest saline lake in the twentieth century. J. Hydrol. 560, 342–353. https://doi.org/10.1016/j.jhydrol.2018.03.034.

Chiang, E., 2022. User guide for processing Modflow version 11: a graphical user interface for MODFLOW, gsflow, modpath, MT3D, PEST, seawat, and ZoneBudget. Simcore Software 334. https://www.simcore.com/files/pm/v11/pm11.0.3pdf.

Condon, L.E., Atchley, A.L., Maxwell, R.M., 2020. Evapotranspiration depletes groundwater under warming over the contiguous United States. Nat. Commun. 11, 873. https://doi.org/10.1038/s41467-020-14688-0.

Danesh-Yazdi, M., Ataie-Ashtiani, B., 2019. Lake Urmia crisis and restoration plan: planning without appropriate data and model is gambling. J. Hydrol. 576, 639–651. https://doi.org/10.1016/j.jhydrol.2019.06.068.

Dehghanzadeh, R., Safavy Hir, N., Shamsy Sis, J., Taghipour, H., 2015. Integrated assessment of spatial and temporal variations of groundwater quality in the eastern area of Urmia Salt Lake Basin using multivariate statistical analysis. Water Resour. Manag. 29, 1351–1364. https://doi:10.1007/s11269-014-0877-7.

Delju, A.H., Ceylan, A., Piguet, E., Rebetez, M., 2013. Observed climate variability and change in Urmia Lake basin, Iran. Theor. Appl. Climatol. 111, 285–296. https://doi.org/10.1007/s00704-012-0651-9.

Derepasko, D., Guillaume, J.H., Horne, A.C., Volk, M., 2021. Considering scale within optimization procedures for water management decisions: balancing environmental flows and human needs. Environ. Model. Software 139, 104991. https://doi.org/10.1016/j.envsoft.2021.104991.

Doble, R.C., Crosbie, R., 2016. Review: current and emerging methods for catchment-scale modelling of recharge and evapotranspiration from shallow groundwater. Hydrogeol. J. 25, 3–23. https://doi.org/10.1007/s10040-016-1470-3.

Doherty, J., 2010. PEST-Model-Independent Parameter Estimation. Version 12. Watermark Computing, Australia, 2010. Available online: http://www.pesthomepage.org/.

Eimanifar, A., Mohebbi, F., 2007. Urmia Lake (northwest Iran): a brief review. Saline Syst. 3 (1), 1–8. https://doi.org/10.1186/1746-1448-3-5.

Fathian, F., Morid, S., Kahya, E., 2015. Identification of trends in hydrological and climatic variables in Urmia Lake basin, Iran. Theor. Appl. Climatol. 119, 443–464. https://doi.org/10.1007/s00704-014-1120-4.

Feizizadeh, B., Abdollahi, Z., Shokati, B., 2022. A GIS-based spatiotemporal impact assessment of droughts in the hyper-saline Urmia Lake basin on the hydro-geochemical quality of nearby aquifers. Rem. Sens. 14 (11), 2516. https://doi.org/10.3390/rs14112516.

Forootan, E., Rietbroek, R., Kusche, J., Sharifi, M.A., Awange, J.L., Schmidt, M., Omondi, P., Famiglietti, J., 2014. Separation of large scale water storage patterns over Iran using GRACE, altimetry and hydrological data. Remote Sens. Environ. 140, 580–595. https://doi.org/10.1016/j.rse.2013.09.025.

Gaiolini, M., Colombani, N., Busico, G., Rama, F., Mastrocicco, M., 2022. Impact of boundary conditions dynamics on groundwater budget in the Campania region (Italy). Water 14 (16), 2462. https://doi.org/10.3390/w14162462.

Gholami, H., Mohammadifar, A., Pourghasemi, H.R., Collins, A.L., 2020. A new integrated data mining model to map spatial variation in the susceptibility of land to act as a source of aeolian dust. Environ. Sci. Pollut. Res. 27, 42022–42039. https://doi.org/10.1007/s11356-020-10168-6.

Gholampour, A., Nabizadeh, R., Hassanvand, M.S., Taghipour, H., Nazmara, S., Mahvi, A.H., 2015. Characterization of saline dust emission resulted from Urmia Lake drying. J Environ Health Sci Eng 13. https://doi.org/10.1186/s40201-015-0238-3, 1-1.

Harbaugh, A.W., 2005. MODFLOW-2005, the US geological survey modular ground-water model: the ground-water flow process. U.S. Geological Survey Techniques and Methods 6-A16; US Department of the Interior. US Geological Survey, Reston, VA, USA, p. 253.

Hassanzadeh, E., Zarghami, M., Hassanzadeh, Y., 2012. Determining the main factors in declining the Urmia Lake Level by using system dynamics modeling. Water Resour. Manage. 26, 129–145. https://doi.org/10.1007/s11269-011-9909-8.

Hill, M.C., 2006. The practical use of simplicity in developing ground water models. Groundwater 44, 775–781. https://doi.org/10.1111/j.1745-6584.2006.00227.x.

Hosseini-Moghari, S.M., Araghinejad, S., Tourian, M.J., Ebrahimi, K., Döll, P., 2020. Quantifying the impacts of human water use and climate variations on recent drying of Lake Urmia basin: the value of different sets of spaceborne and in situ data for calibrating a global hydrological model. Hydrol. Earth Syst. Sci. (4), 1939–1956. https://doi.org/10.5194/hess-24-1939-2020.

Jha, M.K., Chowdary, V.M., 2007. Challenges of using remote sensing and GIS in developing nations. Hydrogeol. J. 15, 197–200. https://doi.org/10.1007/s10040-006-0117-1.

Kakahaji, H., Banadaki, H.D., Kakahaji, A., Kakahaji, A., 2013. Prediction of Urmia Lake water-level fluctuations by using analytical, linear statistic and intelligent methods. Water Resour. Manag. 27, 4469–4492. https://doi.org/10.1007/s11269-013-0420-2.

Karbassi, A., Bidhendi, G.N., Pejman, A., Bidhendi, M.E., 2010. Environmental impacts of desalination on the ecology of Lake Urmia. J Gt Lakes Res 36 (3), 419–424. https://doi.org/10.1016/j.jglr.2010.06.004.

Khazaei, B., Khatami, S., Alemohammad, S.H., Rashidi, L., Wu, C., Madani, K., Kalantari, Z., Destouni, G., Aghakouchak, A., 2019. Climatic or regionally induced by humans? Tracing hydro-climatic and land-use changes to better understand the Lake Urmia tragedy. J Hydrol 569, 203–217. https://doi.org/10.1016/j.jhydrol.2018.12.004.

Kirubakaran, M., Colins, J.J., Samson, S., 2018. MODFLOW based groundwater budgeting using GIS: a case study from Tirunelveli Taluk, Tirunelveli District, Tamil Nadu, India. J Indian Soc Remote Sens 46 (5), 783–792. https://doi.org/10.1007/s12524-018-0761-7.

Li, H.T., Brunner, P., Kinzelbach, W., Li, W.P., Dong, X.G., 2009. Calibration of a groundwater model using pattern information from remote sensing data. J Hydrol 377 (1–2), 120–130. https://doi.org/10.1016/j.jhydrol.2009.08.012.

Lotfirad, M., Esmaeili-Gisavandani, H., Adib, A., 2022. Drought monitoring and prediction using SPI, SPEI, and random forest model in various climates of Iran. J Water Clim Chang 13 (2), 383–406. https://doi.org/10.2166/wcc.2021.287.

Mehrian, M.R., Hernandez, R.P., Yavari, A.R., Faryadi, S., Salehi, E., 2016. Investigating the causality of changes in the landscape pattern of Lake Urmia basin, Iran using remote sensing and time series analysis. Environ. Monit. Assess. 188, 1–3. https://doi.org/10.1007/s10661-016-5456-3.

Micklin, P., 2010. The past, present, and future Aral Sea lakes reservoirs. Res Manage 15 (3), 193–213. https://doi.org/10.1111/j.1440-1770.2010.00437.x.

Mu, Q., Zhao, M., Running, S.W., 2011. Improvements to a MODIS global terrestrial evapotranspiration algorithm. Rem. Sens Environ 115, 1781–1800. https://doi.org/10.1016/j.rse.2011.02.019.

Nasrollahi, H., Shirazizadeh, R., Shirmohammadi, R., Pourali, O., Amidpour, M., 2021. Unraveling the water-energy-food-environment nexus for climate change adaptation in Iran: Urmia Lake Basin case-study. Water 13 (9), 1282. https://doi.org/10.3390/w13091282.

Nikraftar, Z., Parizi, E., Hosseini, S.M., Ataie-Ashtiani, B., 2021. Lake Urmia restoration success story: a natural trend or a planned remedy? J Gt Lakes Res 47 (4), 955–969. https://doi.org/10.1016/j.jglr.2021.03.012.

Ntona, M.M., Busico, G., Mastrocicco, M., Kazakis, N., 2022. Modeling groundwater and surface water interaction: an overview of current status and future challenges. Sci Tot Environ 846, 157355. https://doi.org/10.1016/j.scitotenv.2022.157355.

Pengra, B., 2012. The drying of Iran's lake Urmia and its environmental consequences, UNEP-GRID, sioux falls, UNEP glob. Environ Alert Serv.

Radmanesh, F., Esmaeili-Gisavandani, H., Lotfirad, M., 2022. Climate change impacts on the shrinkage of Lake Urmia. J Water Clim Chang 13 (6), 2255–2277. https://doi.org/10.2166/wcc.2022.300.

Razzagh, S., Sadeghfam, S., Nadiri, A.A., Busico, G., Ntona, M.M., Kazakis, N., 2021. Formulation of Shannon entropy model averaging for groundwater level prediction using artificial intelligence models. Int J Environ Sci Techn 1–8. https://doi.org/10.1007/s13762-021-03793-2.

Rojas, R., Batelaan, O., Feyen, L., Dassargues, A., 2010. Assessment of conceptual model uncertainty for the regional aquifer Pampa del Tamarugal – North Chile. Hydrol. Earth Syst. Sci. 14, 171–192. https://doi.org/10.5194/hess-14-171-2010.

Running, S., Mu, Q., Zhao, M., Moreno, A., 2019. MOD16A2GF MODIS/terra net evapotranspiration gap-filled 8-day L4 global 500m SIN grid V006. NASA EOSDIS Land Processes DAAC. https://doi.org/10.5067/MODIS/MOD16A2GF.006. Available online:

Schmidt, M., Gonda, R., Transiskus, S., 2021. Environmental degradation at Lake Urmia (Iran): exploring the causes and their impacts on rural livelihoods. Geojournal 86 (5), 2149–2163. https://doi.org/10.1007/s10708-020-10180-w.

Shadkam, S., Ludwig, F., van Oel, P., Kirmit, Ç., Kabat, P., 2016. Impacts of climate change and water resources development on the declining inflow into Iran's Urmia Lake. J. Great Lake. Res. 42, 942–952. https://doi.org/10.1016/j.jglr.2016.07.033.

Shah, N., Nachabe, M., Ross, M., 2007. Extinction depth and evapotranspiration from ground water under selected land covers. Groundwater 45, 329–338. https://doi.org/10.1111/j.1745-6584.2007.00302.x.

Sharp, R.P., Glazner, A.F., 1997. Geology Underfoot in Death Valley and Owens Valley. Missoula. Montana Mountain Press, p. 319.

Shepard, D., 1968. A two-dimensional interpolation function for irregularly-spaced data. In: Proceedings of the 1968 23rd ACM national conference, pp. 517–524.

Sima, S., Tajrishy, M., 2013. Using satellite data to extract volume–area–elevation relationships for Urmia Lake, Iran. J Gt Lakes Res 39 (1), 90–99. https://doi.org/10.1016/j.jglr.2012.12.013.

Taheri, M., Emadzadeh, M., Gholizadeh, M., Tajrishi, M., Ahmadi, M., Moradi, M., 2019. Investigating the temporal and spatial variations of water consumption in Urmia Lake River Basin considering the climate and anthropogenic effects on the agriculture in the basin. Agric water manage 213, 782–791. https://doi.org/10.1016/j.agwat.2018.11.013.

Tanji, K.K., 2002. Salinity in the soil environment. In: Salinity: Environment-Plants-Molecules. Springer, Dordrecht, pp. 21–51.

Taravat, A., Rajaei, M., Emadodin, I., Hasheminejad, H., Mousavian, R., Biniyaz, E., 2016. A spaceborne multisensory, multitemporal approach to monitor water level and storage variations of lakes. Water 8 (11), 478. https://doi.org/10.3390/w8110478.

Tourian, M.J., Elmi, O., Chen, Q., Devaraju, B., Roohi, S., Sneeuw, N., 2015. A spaceborne multisensor approach to monitor the desiccation of Lake Urmia in Iran. Remote Sens. Environ. 156, 349–360. https://doi.org/10.1016/j.rse.2014.10.006.

ULRP - Urmia Lake Restoration Program, 2017. Integrated Programme for Sustainable Water Resources Management in Lake Urmia Basin. Project workplan.

Vasilevskiy, P., Wang, P., Pozdniakov, S., Wang, T., Zhang, Y., Zhang, X., Yu, J., 2022. Simulating River/Lake–Groundwater exchanges in arid river basins: an improvement constrained by lake surface area dynamics and evapotranspiration. Rem. Sens. 4 (7), 1657. https://doi.org/10.3390/rs14071657.

Williams, W.D., 1993. The worldwide occurrence and limnological significance of falling water- levels in large, permanent saline lakes. Verh int Ver Limnol 25, 980–983. https://doi.org/10.1080/03680770.1992.11900302.

Williams, W.D., 1996. What future saline lakes? Environ. Times 38, 12–20. https://doi.org/10.1080/00139157.1996.9930999.

Williams, W.D., 2001. Anthropogenic salinisation of inland waters. Hydrobiologia 466, 329–337. https://doi.org/10.1007/978-94-017-2934-5_30.

Yao, Y., Zheng, C., Liu, J., Cao, G., Xiao, H., Li, H., Li, W., 2015. Conceptual and numerical models for groundwater flow in an arid inland river basin. Hydrol. Process. 29, 1480–1492. https://doi.org/10.1002/hyp.10276.

Yazdandoost, F., Moradian, S., Izadi, A., 2020. Evaluation of water sustainability under a changing climate in Zarrineh River Basin, Iran. Water Resour. Manag. 34, 4831–4846. https://doi.org/10.1007/s11269-020-02693-3.

Zhou, Y., Li, W., 2011. A review of regional groundwater flow modeling. Geosci. Front. 2, 205–214. https://doi.org/10.1016/j.gsf.2011.03.003.